Advanced Robotics

ISSN: 0169-1864 (Print) 1568-5535 (Online) Journal homepage: http://www.tandfonline.com/loi/tadr20

Trajectory generation and control of a knee exoskeleton based on dynamic movement primitives for sit-to-stand assistance

Kaveh Kamali, Ali Akbar Akbari & Alireza Akbarzadeh

To cite this article: Kaveh Kamali, Ali Akbar Akbari & Alireza Akbarzadeh (2016) Trajectory generation and control of a knee exoskeleton based on dynamic movement primitives for sit-to-stand assistance, Advanced Robotics, 30:13, 846-860, DOI: 10.1080/01691864.2016.1154800

To link to this article: http://dx.doi.org/10.1080/01691864.2016.1154800

ADVANCED ROBOTICS, 2016
VOL. 30, NO. 13, 846–860
http://dx.doi.org/10.1080/01691864.2016.1154800

RSJ Taylor & Francis
Taylor & Francis Group

FULL PAPER

Trajectory generation and control of a knee exoskeleton based on dynamic movement primitives for sit-to-stand assistance

Kaveh Kamali[a], Ali Akbar Akbari[a] and Alireza Akbarzadeh[b]

[a]Department of Mechanical Engineering, Ferdowsi University of Mashhad, Mashhad, Iran; [b]Center of Excellence on Soft Computing and Intelligent Information Processing, Mechanical Engineering Department, Ferdowsi University of Mashhad, Mashhad, Iran

ABSTRACT

This paper presents a novel control approach for a knee exoskeleton to assist individuals with lower extremity weakness during sit-to-stand motion. The proposed method consists of a trajectory generator and an impedance controller. The trajectory generator uses a library of sample trajectories as the training data and the initial joint angles as the input to predict the user's intended sit-to-stand trajectory. Utilizing the dynamic movement primitives theory, the trajectory generator represents the predicted trajectory in a time-normalized and rather a flexible framework. The impedance controller is then employed to provide assistance by guiding the knee joint to move along the predicted trajectory. Moreover, the human-exoskeleton interaction force is used as the feedback for on-line adaptation of the trajectory speed. The proposed control strategy was tested on a healthy adult who wore the knee exoskeleton on his leg. The subject was asked to perform a number of sit-to-stand movements from different sitting positions. Next, the measured data and the inverse dynamic model of the human-exoskeleton system are used to calculate the knee power and torque profiles. The results reveal that average muscle activity decreases when the subject is assisted by the exoskeleton.

ARTICLE HISTORY
Received 8 May 2015
Revised 20 October 2015
and 12 January 2016
Accepted 18 January 2016

KEYWORDS
Exoskeleton; dynamic movement primitives; assistive control; sit-to-stand

1. Introduction

Sit-to-stand and stand-to-sit movements are essential parts of daily human activity. Standing up is a prerequisite for most human activities, such as walking, running, climbing stairs, etc. Although this maneuver is an easy and routine activity for young and healthy people, it may present considerable difficulty for an older person and for those with a pathology that affects the lower limbs.[1]

Recently, there has been a growing interest in applications of robotic exoskeletons as a solution to assist physically weak people in everyday activities.[2–5] An exoskeleton is a wearable robot, typically with an anthropomorphic configuration that provides a direct transfer of mechanical power to assist or augment the wearer's movement. Lower limb exoskeletons can help elderly and physically dependent people perform their daily activities without the physical assistance of others. Moreover, they can be employed as a rehabilitation device in the recovery period of patients with nervous system and muscular diseases.

When an exoskeleton is utilized to facilitate the wearer's movement, a human intention identification process is often performed during the control process. A common method for human intention identification is to measure biological (e.g. electromyographical) signals.[6,7] However, in these methods, special sensors need to be connected to the user's body, which is not convenient for daily applications. Another strategy for human movement prediction is oscillator-based methods, which are inspired by the rhythm generator inside the spinal cord of humans and other vertebrates (the central pattern generator).[8–10] Zhang and Hashimoto [11] suggested a synchronization-based control strategy that utilizes a neural oscillator model for a motion assistance device. In another study, Ronsse et al. [12] deployed an adaptive oscillator-based controller to provide assistance for a lower-limb exoskeleton, using the learned information from previous motion cycles. Although oscillator-based approaches are successful in estimating the user's intended movement while performing a periodic motion task, they are not suitable for non-periodic motions, such as sit-to-stand and stand-to-sit movements.

Ijspeert et al. [13] proposed a different bio-inspired approach for motion representation and prediction,

CONTACT Ali Akbar Akbari akbari@um.ac.ir

termed *dynamic movement primitives* (DMPs). DMPs are systems of autonomous nonlinear differential equations with the ability to create complex periodic and non-periodic trajectories. The DMP equations are capable of dealing with perturbations. Furthermore, they are independent of timing; thus, the speed of the generated motion is adjustable.[14] Later, Ude et al. [15] proposed a task-specific generalization approach for generating a new trajectory from a database of training trajectories. They labeled each of the training trajectories with a vector that describes the goal of the task. Next, they used DMP equations to encode the new trajectory based on the available training trajectories and the task goal. Using the task goal as input, the method is able to generate a wide range of complex motions; however, it cannot handle training trajectories with different initial conditions.

In this paper, Ude's approach is extended to allow prediction of new trajectories based on a library of non-periodic training trajectories with different initial conditions. The proposed method is then employed to predict human sit-to-stand movement for a given initial sitting position. The predicted trajectory is used as the reference trajectory of the knee exoskeleton. An impedance controller is designed to calculate the required torques for assisting the wearer to move along the predicted trajectory while allowing him/her to partly control the speed of the sit-to-stand movement. The trajectory generation method introduced in this paper needs to obtain training data from the same subject who wants to use the exoskeleton. In this study, it is assumed that, with the supervision of a physiotherapist, the training data and the body dimension data of the subject can be obtained under controlled conditions. In this way, the training data will be the best trajectories for the specific user. Although this procedure requires a number of training sessions, it makes the exoskeleton to efficiently work for the specific user for his/her whole life.

The contributions of this paper include:

(1) Introduction of a trajectory generation method for synthesizing new trajectories from a library of training trajectories using a desired initial condition vector as the input.
(2) Utilization of the DMP theory in the trajectory generation process to represent the predicted trajectory in a time-normalized and rather a flexible way.
(3) Employment of the proposed method to generate the reference trajectory of the knee exoskeleton for sit-to-stand movement based on the human joint angles in the sitting position.
(4) Use of the human-exoskeleton interaction forces as feedback for on-line adaptation of the trajectory speed.

The rest of this paper is organized as follows. In Section 2, the structure of the knee exoskeleton is described, and a 2D dynamic model of the human body and the exoskeleton is presented. Section 3 introduces the trajectory generation method. The application of the method proposed in Section 3 for prediction of the human sit-to-stand motion is discussed in Section 4. Section 5 provides a description of the controller implementation and the experimental setup. Experimental results and discussion are presented in Section 6. Finally, conclusions and future works are given in Section 7.

2. Dynamic model of the human-exoskeleton system

A prototype powered knee exoskeleton (FUM-KneeExo) has been designed and developed at the Ferdowsi University of Mashhad robotic laboratory (FUM Robotic Lab) to assist human subjects during sit-to-stand movement (Figure 1(a)). This device is powered by a linear series elastic actuator (LSEA), which was constructed in FUM Robotic lab (Figure 1(b)). The LSEA provides relatively low output mechanical impedance in the exoskeleton actuation system, which results in more accurate and robust control of human–robot interaction forces. This actuator transfers the rotary movement of the servo motor to the linear movement using a ball screw. Power is then transmitted to the output through a spring set. A magnetic linear encoder measures the deflection of the spring set, which is used to estimate the output force of the LSEA.

FUM-KneeExo consists of three articulated links and the LSEA. These links are connected by one revolute joint for the knee flexion/extension motions and a passive revolute joint for ankle plantar/dorsi-flexion motions. An encoder measures the rotation of the ankle joint, which is used as an input for the trajectory prediction system. The LSEA is connected to the upper (thigh) and middle (shank) links to provide the required power for assisting the knee flexion–extension movement. One strap on each link of the exoskeleton is used to attach the mechanism to the user. The foot link is designed to transfer the human and exoskeleton weight to the ground. Additionally, four force sensors are embedded in the foot part to measure the ground reaction forces. Table 1 shows the specifications of the LSEA that is utilized in this study.

Dynamic analysis of the human-exoskeleton model is essential for the exoskeleton's trajectory generation

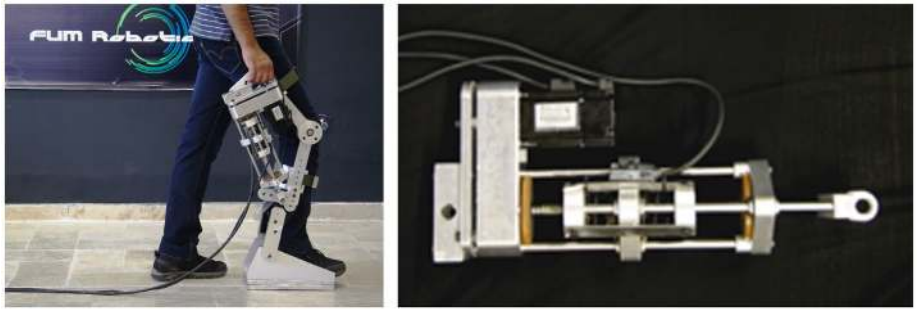

Figure 1. (a) FUM-KneeExo, the powered knee exoskeleton developed in the FUM Robotic Lab; (b) the LSEA.

Table 1. Specifications of the LSEA.

Gear ratio (linear movement/motor rotation)	2.5 mm/rot
Spring stiffness	50,000 N/m
Max output force	1000 N
Max linear speed	125 mm/s

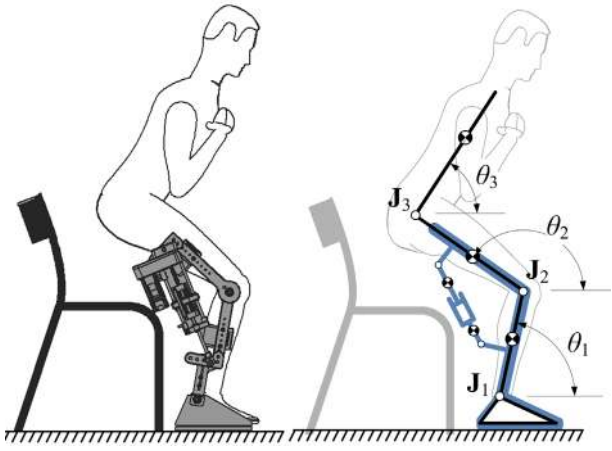

Figure 2. Kinematic model of the human-exoskeleton system in the sagittal plane.

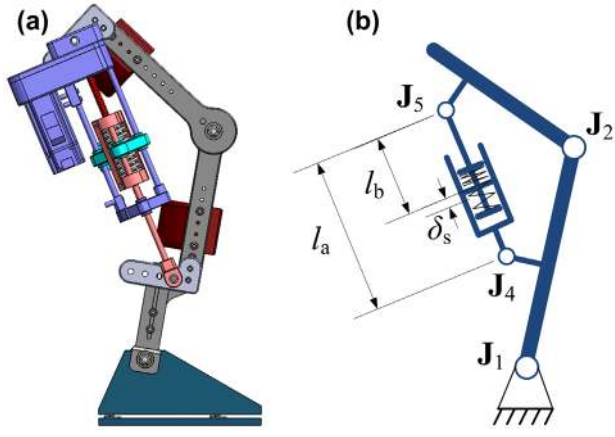

Figure 3. (a) Solid model and (b) kinematic model of FUM-KneeExo.

and control system. According to [16,17], humans commonly rise from sitting in an essentially sagittal symmetric manner; consequently, using a two-dimensional model is rational for sit-to-stand movement. During sit-to-stand movement, the human body can be approximated structurally by three rigid links: shank, thigh, and HAT (Head–Arms–Trunk).[18] The robot moves in parallel to the skeleton of the subject; therefore, the exoskeleton links are considered to be rigidly connected to the human limbs. The shank link of the model is representative of the shanks of the human body. The thigh link represents the human thighs. Thus, the mass of each thigh and shank link of the model is considered double of each thigh and shank of the human body.

The combination of the human body and FUM-KneeExo, can be modeled as a six-link mechanism with a close chain in the sagittal plane. The mechanism has four degrees-of-freedom (DOFs) including ankle rotation, knee rotation, hip rotation, and one DOF inside of the LSEA mechanism. The kinematic model of the entire system is shown in Figure 2. Moreover, Figure 3 illustrates the kinematic model of FUM-KneeExo.

The Lagrangian formulation is used to derive the dynamic equations of motion of the system. The configuration of this dynamic system can be described by five generalized coordinates, $q_k (k = 1, \ldots, 5)$, as follows,

$$\begin{cases} q_1 = \theta_1 \\ q_2 = \theta_2 - \theta_1 \\ q_3 = \theta_3 - \theta_2 \\ q_4 = l_b \\ q_5 = \delta_s \end{cases} \quad (1)$$

where l_b represents the linear movement of the ball screw, and δ_s is the deflection of the spring in the LSEA. This system is subject to one geometric constraint and thus possesses 5–1 = 4 DOFs. Therefore, one of the generalized coordinates is dependent. Here, the spring deflection (q_5) is considered as the dependent generalized coordinate.

The time derivative of the geometric constraint can be presented by the following equation,

$$\sum_{k=1}^{5} \alpha_k \dot{q}_k = 0 \tag{2}$$

Using the constraint equation coefficients α_k, the equations of motion of this system can be formulated based on Lagrange's equations,

$$\frac{d}{dt}\left(\frac{\partial L}{\partial \dot{q}_k}\right) - \frac{\partial L}{\partial q_k} = \left(F_k\right)_{nc} + \lambda \alpha_k, \quad (k = 1, \ldots, 5) \tag{3}$$

$$L = K - V \tag{4}$$

where L is the Lagrangian, K is the kinetic energy, and V is the potential energy of the system. The generalized non-conservative force/torque associated with q_k is indicated by $\left(F_k\right)_{nc}$, while λ is the Lagrange multiplier related to the constraint equation. For this system, the kinetic energy and potential energy functions can be obtained as follows,

$$K = \sum_{i=1}^{6} \frac{1}{2} J_i \omega_i^2 + \sum_{i=1}^{6} \frac{1}{2} m_i ||\mathbf{v}_i^2|| \tag{5}$$

$$V = \sum_{i=1}^{6} m_i h_i g + \frac{1}{2} k \cdot \delta_s^2 \tag{6}$$

where $\mathbf{v}_i$, h_i, and ω_i are the velocity vector, the height, and the angular velocity of the *ith* link, respectively. Moreover, m_i and J_i indicate the mass and inertia of the *i*th link.

Solving the complete set of the constraint equation, Equation (2), and Equation (3) leads to the inverse dynamics equations of the entire exoskeleton-human system as follows,

$$\mathbf{F} = \mathbf{M}(\mathbf{q})\,\ddot{\mathbf{q}}^{\boldsymbol{a}} + \mathbf{C}(\mathbf{q},\ \dot{\mathbf{q}})\,\dot{\mathbf{q}}^{\boldsymbol{a}} + \mathbf{G}(\mathbf{q}) \tag{7}$$

where $\mathbf{q}^{\boldsymbol{a}} = [q_1, \ldots, q_4]^T$ is the independent generalized coordinates vector. $\mathbf{M}(\mathbf{q})$ is a 4×4 inertia matrix and $\mathbf{C}(\mathbf{q}, \dot{\mathbf{q}})$ is a 4×4 Coriolis and centripetal matrix. $\mathbf{G}(\mathbf{q})$ is a 4×1 vector representing gravitational forces. $\mathbf{F}$ is the 4×1 generalized force vector associated with the independent generalized coordinates, which is defined as,

$$\mathbf{F} = \begin{bmatrix} \tau_{\text{ankle}} \times 2 \\ \tau_{\text{knee}} \times 2 \\ \tau_{\text{hip}} \times 2 \\ F_b \end{bmatrix}, \tag{8}$$

where τ_{ankle}, τ_{knee}, and τ_{hip} are the torques applied by the human on the ankle, knee and hip joints of each leg, respectively. F_b represents the applied force by the linear actuator (ball screw) in the LSEA. The spring force (F_s) is associated with the dependent generalized coordinate q_5 and can be obtained by the following relation,

$$F_s = k_s \delta_s \tag{9}$$

where k_s is the spring stiffness. In this study, the exoskeleton is only worn on one leg of the subject. Although it may induce some undesirable asymmetric motion, the errors are negligible and the sit-to-stand movement still can be considered as a planar movement.

3. Generalization of non-periodic movements using DMPs

As mentioned earlier, Ude et al. [15] introduced a task-specific generalization approach for non-periodic and periodic movements based on the DMP theory. This approach uses a database of training trajectories to synthesize a new trajectory according to the desired task goal. To this end, they labeled each training trajectory with parameters that describe the characteristics of the task (goal of the task). In Ude's approach, the entire training trajectories are supposed to start from the same initial position. In this section, the above-mentioned method is additionally extended to take into account different initial conditions of the training trajectories.

3.1. Theoretical fundamentals of DMPs

The theoretical fundamentals of the DMPs are introduced by Ijspeert et al. [13,19] They defined the DMPs as a set of autonomous differential equations having well-defined attractor properties. As a basic point-attractive system, Schaal et al. [14] proposed a second-order system of differential equations as follows,

$$\eta \dot{z} = \alpha_z\left(\beta_z\left(y_{\text{goal}} - y\right) - z\right) + f(x) \tag{10}$$

$$\eta \dot{y} = z \tag{11}$$

For simplification, only a single DOF (y) is considered in the above equations. The parameters y_{goal} and η are final destination and the time constant of the trajectory, respectively. Selecting the proper value for the constant parameters α_z, β_z, and $\eta > 0$(e.g. $\alpha_z = 4\beta_z$) will lead this system to a particular attractor point at $z = 0$, $y = y_{\text{goal}}$. Throughout the paper, the values of $\alpha_z = 25$and $\beta_z = 25/4$ are used. The function $f(x)$ is a linear combination of radial-basis

functions [14], which makes it possible to approximate any non-periodic trajectory by integrating Equations (10) and (11). In this paper, $f(x)$ is defined as,

$$f(x) = \frac{\sum_{i=1}^{M} w_i \Psi_i(x)}{\sum_{i=1}^{M} \Psi_i(x)} x, \quad \Psi_i(x) = \exp\left(-\sigma_i (x - c_i)^2\right) \tag{12}$$

where $c_i, i = 1, \ldots, M$ are the centers of the M radial basis functions that are distributed along the x-axis in the range of 0 to 1, and $\sigma_i > 0$. The parameter x is used as a phase variable in Equation (12), instead of time, to make the equations independent of time. This variable is generated through the following dynamic equation,

$$\eta \dot{x} = -\alpha_x x \tag{13}$$

This equation is called 'leaky integrator' [14], which is a basic dynamic system for creating a point attractor. In this study, the constant value of $\alpha_x = 25/3$ and the initial condition of $x(0) = 1$is considered for the above equation. An on-line or off-line optimization should be undertaken to determine the shape parameters w_i so that the produced trajectory by integrating Equations (10), (11), and (13) can accurately fit the training trajectory. Trajectory speed can be tuned on-line by modifying η without affecting the trajectory shape. It should be considered that, for all DOFs, the time constant η must be the same.

Schaal et al. [14] proposed a supervised learning method to find w_i. In this method, it is supposed that a sample trajectory y_s, $\dot{y}_s$, and $\ddot{y}_s$, is given. Based on this information, they proposed the following target for f:

$$f_{\text{target}}(t_j) = \eta^2 \ddot{y}_s(t_j) + \alpha_z \eta \dot{y}_s(t_j) - \alpha_z \beta_z \left(y_{\text{goal}} - y_s(t_j)\right), j = 1, \ldots, T \tag{14}$$

where T is the number of the sample points on the trajectory. Considering the following equations:

$$\mathbf{F}_{\text{target}} = \begin{bmatrix} f_{\text{target}}(t_1) \\ \vdots \\ f_{\text{target}}(t_T) \end{bmatrix} \tag{15}$$

$$\mathbf{w} = \begin{bmatrix} w_1 \\ \vdots \\ w_M \end{bmatrix} \tag{16}$$

$$\mathbf{X} = \begin{bmatrix} \frac{\Psi_1(x_1)}{\sum_{i=1}^{M} \Psi_i(x_1)} x_1 & \cdots & \frac{\Psi_M(x_1)}{\sum_{i=1}^{M} \Psi_i(x_1)} x_1 \\ \vdots & \vdots & \vdots \\ \frac{\Psi_1(x_T)}{\sum_{i=1}^{M} \Psi_i(x_T)} x_T & \cdots & \frac{\Psi_M(x_T)}{\sum_{i=1}^{M} \Psi_i(x_T)} x_T \end{bmatrix}, \tag{17}$$

they indicated that minimizing the term $\mathbf{Xw} - \mathbf{F}_{\text{target}}$ leads to the optimum shape parameters w_i of the DMP equations that fit the training trajectory (off-line training). Therefore, the least-squares method can be used to calculate the shape parameters w_i.

3.1.1. Illustrative example of off-line training of a DMP system

In this section, an illustrative example of off-line training of a one-dimensional DMP system is presented. A three-segment fifth-order polynomial trajectory is considered as the training trajectory (y_s) as follows,

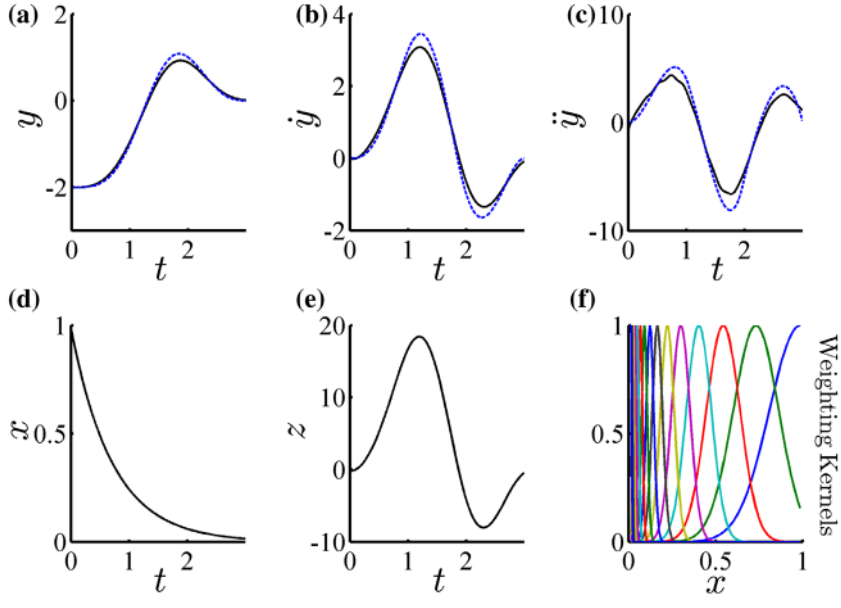

Figure 4. Approximation of a three-segment fifth-order polynomial trajectory with the DMP equations.

$$y_s(t) = \begin{cases} -t^5 + 2t^4 - 2, & 0 \le t < 1 \\ \frac{3}{2}t^5 - \frac{19}{2}t^4 + \frac{41}{2}t^3 - \frac{35}{2}t^2 + 7t - 3, & 1 \le t < 2 \\ -\frac{t^5}{2} + \frac{9}{2}t^4 - \frac{25}{2}t^3 + \frac{9}{2}t^2 + 27t - 27, & 2 \le t \le 3 \end{cases} \quad (18)$$

Figure 4 illustrates the off-line training results of the DMP equations. The goal is set to $y_{\text{goal}} = 0$, and the initial conditions are set to $x(0) = 1$ and $y_{t=0} = -2$. Moreover, the time constant is set to $\eta = 6$. As is depicted in the Figure 4(f), the forcing term consists of $M = 15$ radial-basis functions, which are exponentially distributed along x. The Figure 4(a–c) illustrates the position, velocity, and acceleration of the training and the approximated trajectories, respectively. The results reveal that the trajectory produced by the DMP equations (solid lines) mostly fits the training trajectory (dashed lines). Figure 4(d and e) show the variables x and z vs. time.

3.2. Trajectory generation based on initial conditions

In some applications, such as sit-to-stand movement, different initial conditions lead to different shapes and timings of trajectories. In this section, a methodology for generalization of a library of training trajectories based on the initial condition vector is presented. In this regard, an optimization method is suggested to estimate the shape parameters and the time constant of the DMP equations for a given initial condition vector. This DMP system synthesizes a new trajectory starting from the desired initial condition vector.

Consider a set of training trajectories with the same goal but different initial conditions. For generalization of these sample trajectories, first, the initial condition vector and the time constant of each trajectory should be extracted. The set of training data associated with their initial conditions and timing can be defined as,

$$Z = \left\{ y_s^k\left(t_{k,j}\right),\ \dot{y}_s^k\left(t_{k,j}\right),\ \ddot{y}_s^k\left(t_{k,j}\right); (\mathbf{I}_k, \eta_k) | k = 1, \ldots, N, \quad j = 1, \ldots, T_k \right\} \quad (19)$$

where $y_s^k\left(t_{k,j}\right), \dot{y}_s^k\left(t_{k,j}\right)$ and $\ddot{y}_s^k\left(t_{k,j}\right)$ are the positions (displacements or angles), velocities, and accelerations of the kth training trajectory at the jth sample point, N is the number of training trajectories, and T_k is the number of sampling points on each trajectory. Moreover, $\mathbf{I}_k$ and η_k indicate the initial condition and time constant of the kth trajectory, respectively. The initial condition vector of the kth trajectory is defined as,

$$\mathbf{I}_k = [y_s^k(t_{k,1}),\ \dot{y}_s^k(t_{k,1}),\ \ddot{y}_s^k(t_{k,1})]^T \quad (20)$$

To specify a DMP equation set that synthesizes the desired trajectory corresponding to the desired vector of the initial condition, the desired shape parameter vector $\mathbf{w}_d$ and time constants η_d need to be estimated. Therefore, the function $\mathfrak{F}(Z)$ can be defined as a relationship between the initial condition vector and both the shape parameter vector $\mathbf{w}$ and the time constant η as follows,

$$\mathfrak{F}(Z): \mathbf{I} \rightarrow (\mathbf{w}, \eta) \quad (21)$$

The relation $\mathfrak{F}(Z)$ can be found via an optimization procedure. The optimization goal is to determine the optimum shape parameter vector ($\mathbf{w}_d$) and time constant (η_d) of the DMP equations so that the solution trajectory is as similar as possible to those training trajectories that their initial condition ($\mathbf{I}_k$) is near to the desired initial condition ($\mathbf{I}_d$). Here, locally weighted regression [19] is employed to determine the optimum DMP parameters by minimizing the following fitness function,

$$\mathcal{H} = \sum_{k=1}^{N} \left(\mathbf{X}_k \mathbf{w} - \mathbf{F}_k^2 + \left(\eta - \eta_k\right)^2 \right) \times k\left(d(\mathbf{I}_d, \mathbf{I}_k)\right) \quad (22)$$

with respect to $\mathbf{w}$ and η. In this equation, N represents the number of training trajectories, and the functions k and d are defined as,

$$k(d) = \begin{cases} \left(1 - |d|^3\right)^3, & \text{if } |d| < 1 \\ 0, & \text{otherwise} \end{cases} \quad (23)$$

$$d\left(\mathbf{I}_d, \mathbf{I}_k\right) = \mathbf{D} \times (\mathbf{I}_d - \mathbf{I}_k), \quad \mathbf{D} = \text{diag}\left(\frac{1}{\gamma_i}\right),\ \gamma_i > 0 \quad (24)$$

where γ_i is a normalization coefficient, which is defined as,

$$\gamma_i = \max_{j=1,\ldots,N} \min_{k=1,\ldots,N} \left\{ \left| I_{j,i} - I_{k,i} \right| \right\} \quad (25)$$

The kernel function k which is used here is proposed by Ude et al. [15]. This function determines the influence of each training trajectory on the estimation of the synthesized trajectory. This kernel function ignores the training trajectories which their initial conditions are too far from the desired initial condition. This reduces the computational complexity of the generalization problem. Here, a cubic norm is chosen to have continuous first and second derivatives.

Table 2. The experimental conditions for sit-to-stand generalization.

Chair height (cm)	Foot positions (cm)
40	−10, −7, −4, 0, 4
43	−10, −7, −4, 0, 4
46	−10, −7, −4, 0, 4
49	−10, −7, −4, 0, 4

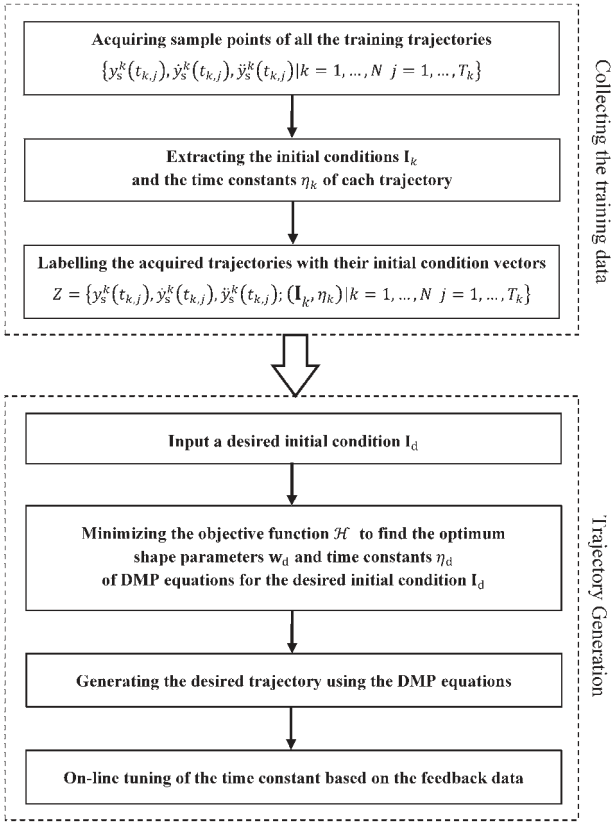

Figure 5. The procedure of the proposed trajectory generation.

Using this training method, each training trajectory is weighted based on the distance between its initial condition vector and the desired initial condition vector. Therefore, adjacent training trajectories affect the result more. The optimization process of minimizing the $\mathcal{H}$ function will lead to a least-squares problem that can be solved by standard algebra methods.

In Section 5, an adaptation strategy will be proposed that tunes the time constant of the predicted trajectory to be synchronized with the user's intended moving speed. The entire procedure of the proposed trajectory generation is described in Figure 5.

4. Generalization of sit-to-stand movement: a case study

Initial foot position and seat height are considered important factors for ease of standing up. According to [20,21], human joint trajectories and muscle activity patterns are considerably different under various initial foot conditions. Therefore, it is reasonable to utilize the proposed trajectory generation method to predict the sit-to-stand trajectories for a given initial sitting position.

As a case study, a set of experiments on a single adult male, with a mass of 70 kg and a height of 1.72 m, is conducted. The parameters specifying the sitting position are, in this case, the initial angles of the ankle and the knee joints, which correspond to the initial seat height and the foot positions. The subject performed a sequence of sit-to-stand movements for four descending seat heights. For each seat height, five sit-to-stand movements with five different foot positions were performed. Multiple experiments are performed for each sitting position. Among them, three best measurements are selected and averaged. The experimental conditions including chair heights and feet positions are shown in Table 2. The foot positions are measured relative to the vertical position of the shank. The kinematic data of these experiments were collected in the motion laboratory of the Sport Science Research Institute of Iran, equipped with a Raptor-E Digital Real-Time Motion Analysis System (Figure 6). During the experiments, two AMTI force plate were placed underneath the subject's feet to measure the ground reaction forces. In the process of standing from a chair, when the buttocks lose contact with the chair, the horizontal component of the foot–ground reaction force increases suddenly. This instance is termed as seat-off. The subject is asked to rise from the chair with an approximately same speed for all initial sitting positions. The measured sit-to-stand trajectories are then synchronized based on the seat-off instance. Figure 7(a) illustrates the paths of the shoulder, hip, knee, and ankle during the sit-to-stand task for four different seat heights. The collected motion data and the 2D kinematic model of the human body are used to calculate the ankle, knee, and hip joint angles during sit-to-stand movement. Additionally, the angular velocities and the angular accelerations are calculated from the time-derivative of the filtered angular positions (a first-order Butterworth filter with a 20-Hz cut-off frequency). Figure 7(b–d) illustrate the trajectories of ankle, knee, and hip joint angles during the sit-to-stand interval for four different seat heights and a same foot position.

The subject's knee and ankle angles do not change before the seat-off. Therefore, it is reasonable to consider the instance of seat-off as the initiation of the training trajectories. Because the initial hip angle cannot be measured during the control process, it is not considered as an element of the initial condition vector. Moreover, at the instance of seat-off, angular velocity and acceleration of knee and ankle are negligible. Consequently, in this study, the initial condition vector of sit-to-stand ($\mathbf{I}$) is a two-dimensional vector including the angles of the knee

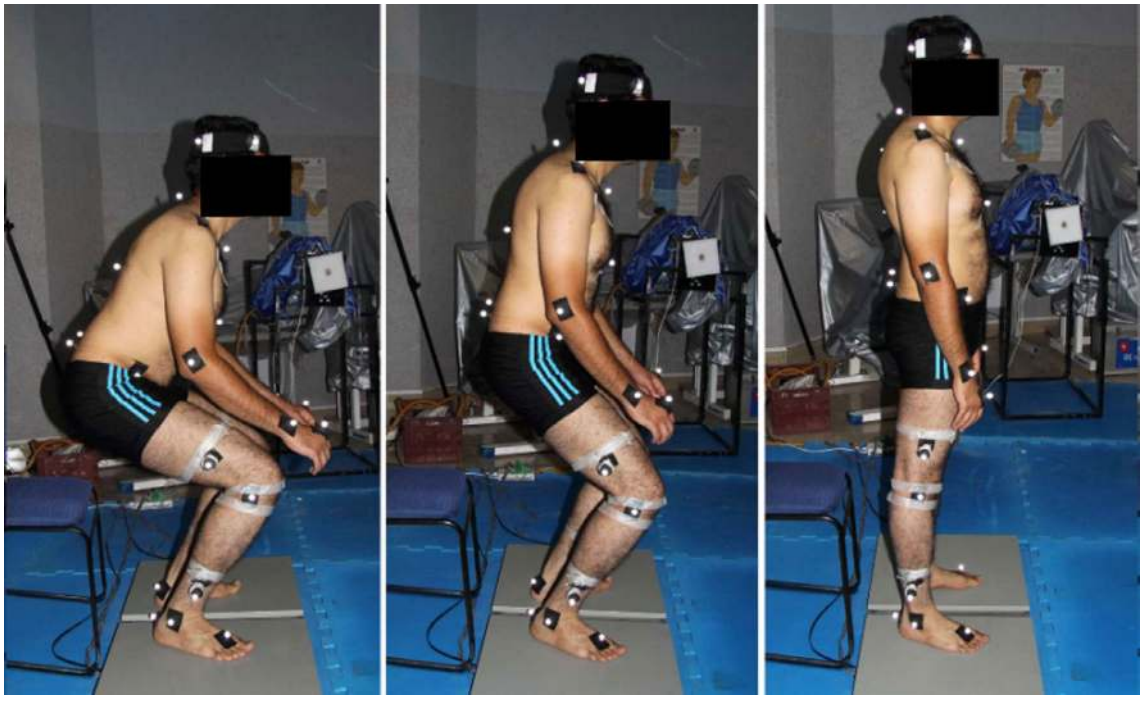

Figure 6. Snapshots from the motion analysis procedure of sit-to-stand trials.

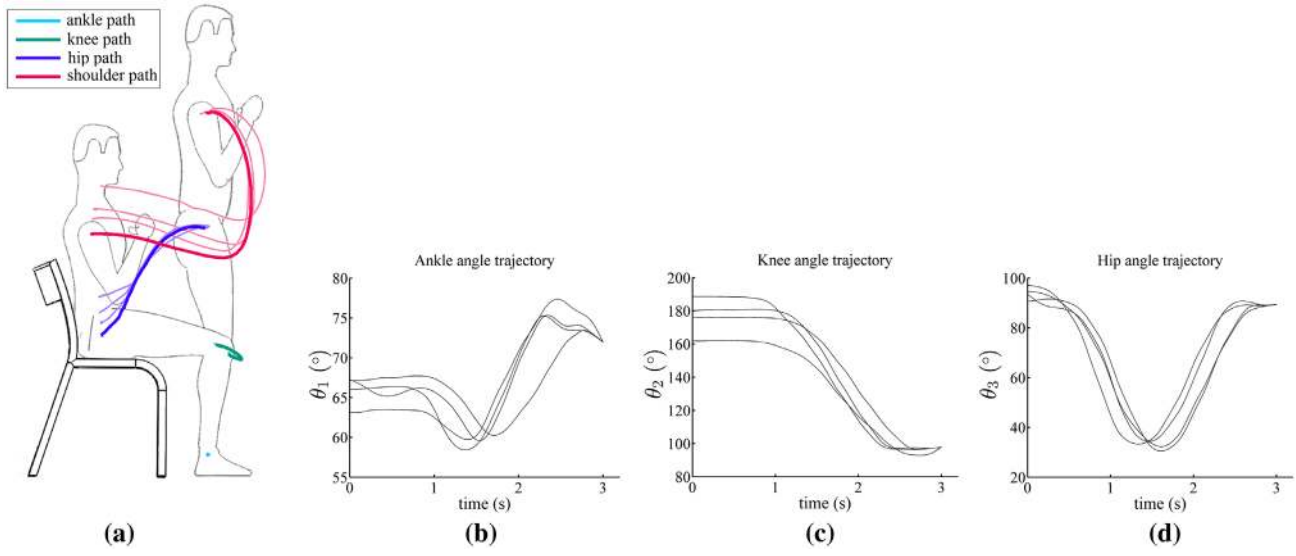

Figure 7. (a) Path of the shoulder, hip, knee, and ankle during the sit-to-stand task for four different seat heights; (b, c, d) angle profiles of the ankle, knee, and hip joints during sit-to-stand movements for four different seat heights.

and ankle joints at the moment of seat-off. For both the dimensions value of x is set to $x(0) = 1$, and the forcing term consists of $M = 25$ radial-basis functions, which are exponentially distributed along x. Therefore, for each dimension a separate 25-dimentional vector of shape parameters ($\mathbf{w}$) must be calculated. The other constant parameters (α_z, β_z, and α_x) are same as Section 3.1.

Following the trajectory generation algorithm (Figure 5), the goal, the initial condition ($\mathbf{I}$), and time interval (η) of each sample trajectory are extracted. Next, for any desired initial sitting position, the fitness function (Equation (22)) is minimized to calculate the desired shape parameters ($\mathbf{w}_d$) and time interval (η_d) of the DMP model. The results of generalization of seat-to-stand trajectories are illustrated in Figure 8. In this figure, the initial conditions related to the training trajectories are indicated with small triangles, and the initial conditions of the generated trajectories are represented with small squares. The results reveal an

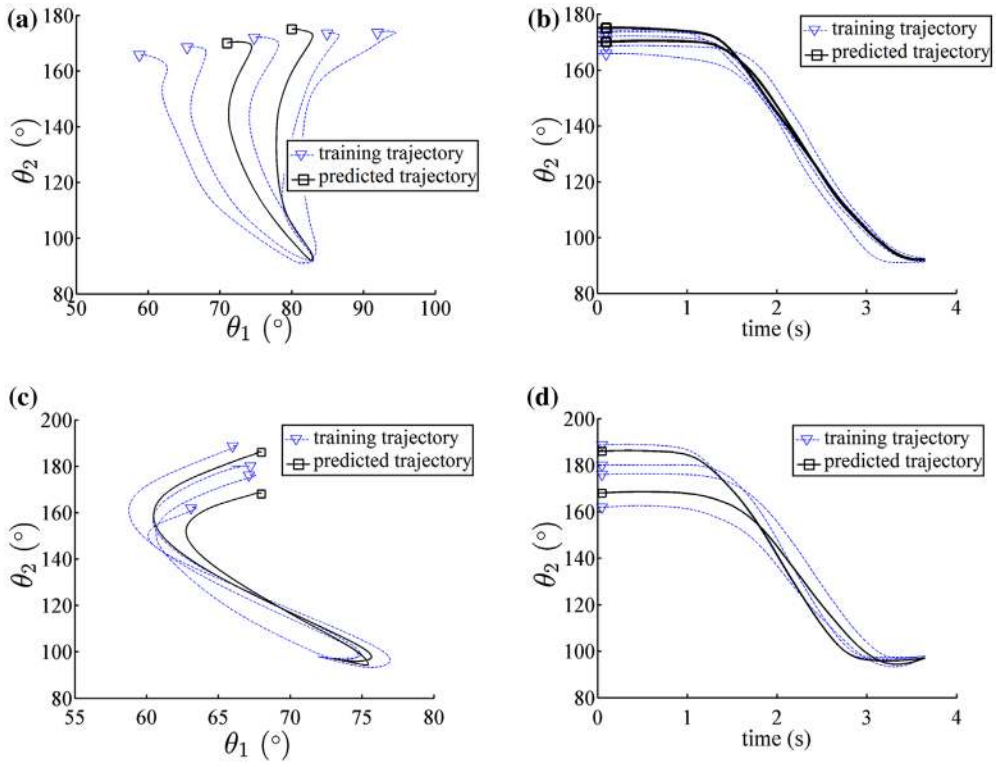

Figure 8. Generalization of sit-to-stand movement. Graphs (a) and (c) illustrate the knee angle vs. the ankle angle for different foot positions and different seat heights, respectively. Graphs (b) and (d) illustrate the knee angle with respect to time for different foot positions and different seat heights, respectively.

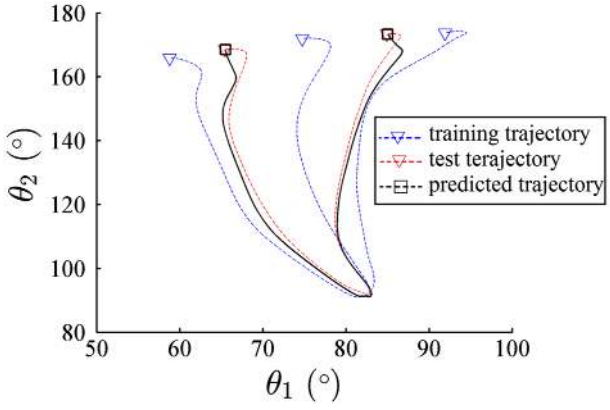

Figure 9. Quantitative evaluation of the proposed generalization method.

outstanding similarity between the shape of the generated trajectories (solid lines) and the nearby training trajectories (dashed lines).

In Figure 9, quantitative evaluation of the predicted trajectory is presented. In this figure, three trajectories (blue dashed lines) are used as the training and two trajectories (red dashed lines) as the test trajectories. In order to evaluate the proposed trajectory generation method, the generated trajectories (solid lines) are calculated with the same initial conditions as the initial conditions of the test trajectories. The results show that the generated trajectories practically fit the test trajectories. Therefore, the proposed method can effectively predict the sit-to-stand movements of human.

5. Controller implementation

FUM-KneeExo aims to help the wearer to move along the predicted sit-to-stand trajectory while letting him/her, to some extent, conduct the movement. To this end, an impedance control is employed to apply the required driving force to the exoskeleton.

5.1. Impedance controller

The controller used in this study is composed of an inner force feedback loop and an outer impedance control loop. Additionally, a gravity compensator and an inverse dynamic model are used to estimate the gravitational and dynamic forces/torques. The force loop is designed to track the desired force at the output of the LSEA. The outer control loop creates a relationship between the position of the LSEA and the force it applies. The outer control loop calculates the reference force based on a desired impedance model, which characterizes a virtual

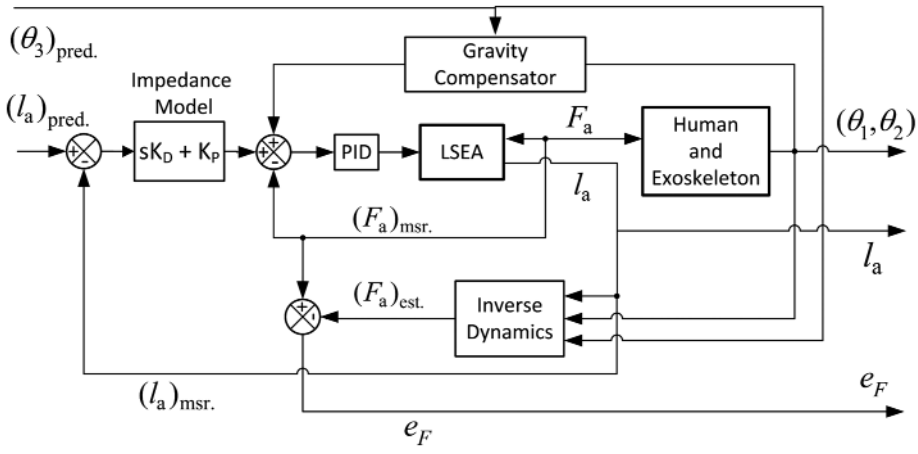

Figure 10. The block diagram of the impedance controller implemented on FUM-KneeExo.

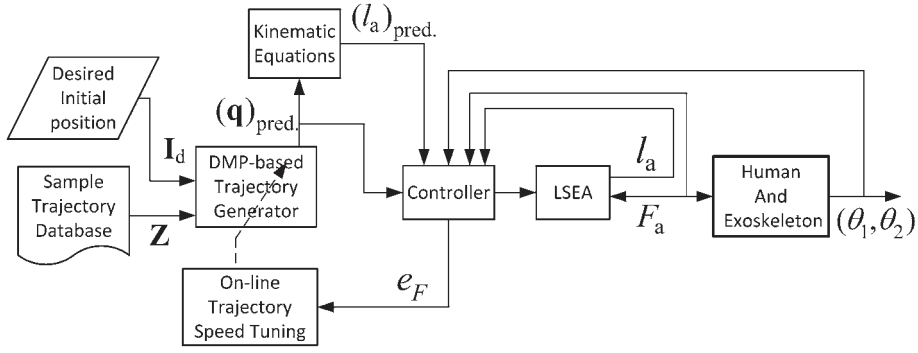

Figure 11. Overall structure of the proposed control architecture for FUM-KneeExo.

spring stiffness and a virtual damper. The impedance control architecture is illustrated in Figure 10. In this figure, $(l_a)_{pred.}$ and l_a represent the predicted and measured length of the LSEA. Using kinematic model of the human and exoskeleton, $(l_a)_{pred.}$ is calculated from the predicted knee angle. Moreover, the measured actuator force is depicted by $(F_a)_{msr.}$ which is approximately equal to the measured force of the LSEA's spring ($(F_s)_{msr.} = k_s\delta_s$). The inner force controller includes a PID controller which is tuned by Ziegler–Nichols method. In order to avoid instability a low pass filter for the derivative term is used to limit the high frequency gain and noise.

An online adaptation process is used to synchronize the DMP trajectory speed with the user's intended speed. In this process, the inverse dynamic model is used to estimate the LSEA force ($(F_a)_{est.}$). The force error e_F is then calculated by subtracting the estimated force from the measured force ($(F_a)_{msr.}$) of the LSEA. Negative values of e_F indicate the user's intention to speed the movement up, and positive values represent the user's intention to slow it down. Therefore, the following adaptation equation is suggested for on-line tuning of the time constant,

$$\dot{\eta} = \zeta e_F \tag{26}$$

where ζ represents the adaptation rate. Figure 11 illustrates the complete architecture of the trajectory generation and control of FUM-KneeExo. The trajectory generator block uses the training data and the initial value of the knee and ankle angles to generate the reference trajectory. Here, seat-off is considered as the initiation of the sit-to-stand trajectories; therefore, the initial condition vector can be obtained from the value of the knee and ankle angle at this moment. In this regard, the ground reaction force, which is measured by foot force sensors, is used to detect the instance of seat-off.

5.2. The hardware

The control hardware of FUM-KneeExo consists of a host desktop PC, a real-time target desktop PC, a data acquisition I/O card, and the servo motor driver. The controller algorithms are developed on the Host PC. The xPC toolbox of the MATLAB software then creates an executable file to be used for real-time control on the target PC. The target PC is connected to the host PC and the data acquisition I/O card through a LAN. The I/O card used for this study is a multifunctional digital I/O, analog I/O, and

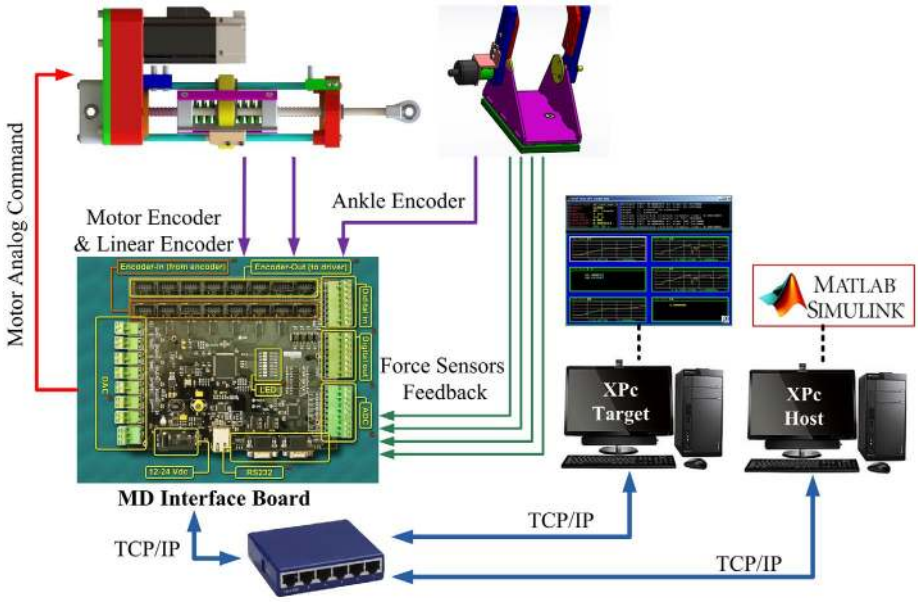

Figure 12. The experimental setup of the proposed controller.

Figure 13. Snapshots from the sit-to-stand movement trials with the assistance of FUM-KneeExo.

counter card that has been created in the FUM Robotic Lab. Figure 12 depicts the overall architecture of the hardware/software of the control system.

6. Experimental results and discussion

To evaluate the proposed assistive control method, a set of experiments were adopted with the same individual who participated in the case study described in Section 4. The collected kinematic data are used as the training database for the trajectory generation process. Two sets of experiments were performed. In the first set, the subject was instructed to do sit-to-stand movements from five different foot positions with the same seat height while wearing FUM-KneeExo on his leg (see Figure 13). In the second experiment set, the subject rose from four different seat heights with the same foot position. For each sitting position, ten consecutive sit-to-stand movements were performed. During all of the experiments, the exoskeleton was operating under the proposed control system.

To assess the exoskeleton's performance, the power and torque profiles of the user's knee for the condition of being assisted by the exoskeleton (*assisted* condition) are compared with the condition in which the user did not wear the exoskeleton (*unassisted* condition). The inverse dynamic model introduced in Section 2 (Equation 7)

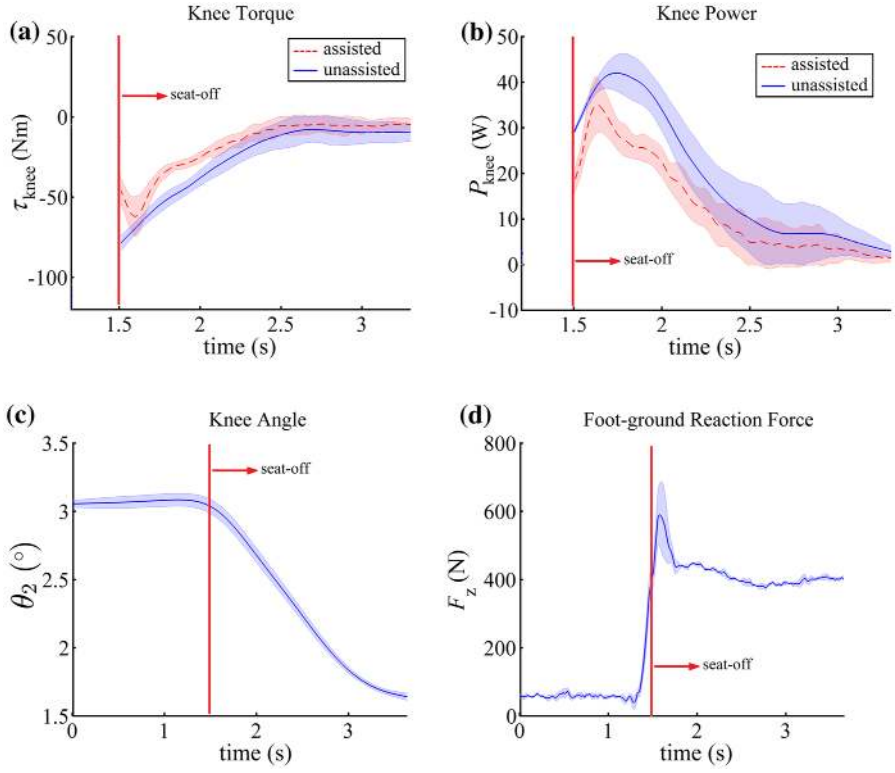

Figure 14. The intrasubject mean and ±1 SD profiles of (a) the knee torque; (b) the knee power; (c) the knee angle; (d) the ground reaction force during sit-to-stand movement.

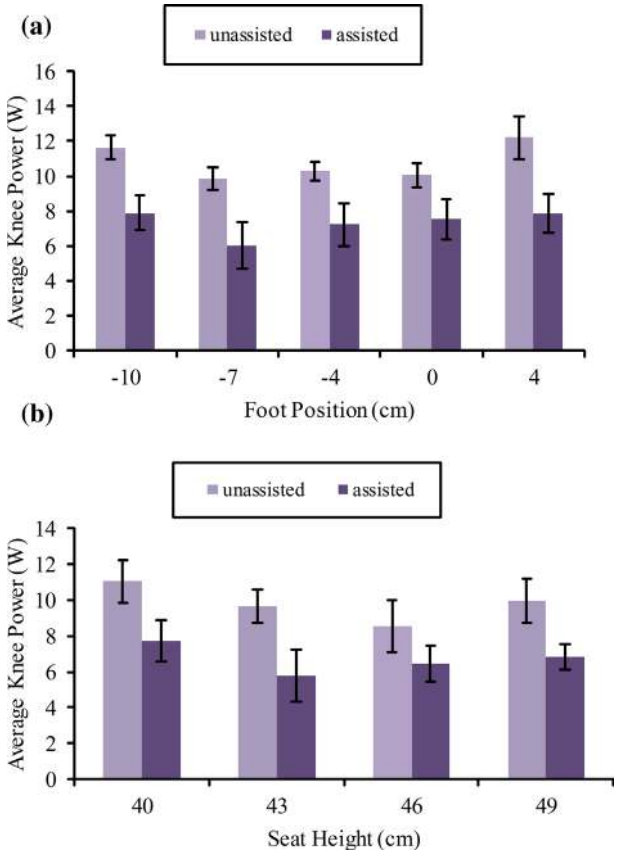

Figure 15. Average of knee power for assisted/unassisted conditions across (a) different foot positions and (b) different seat heights.

is employed to calculate the torque profiles, which are needed to realize the measured hip, knee, and ankle rotations. For the *unassisted* condition, the actuator force and the mass and moment of inertia of the exoskeleton parts are set to zero in the inverse dynamics equation. The mass and moment of inertia of the human model segments are estimated from the anthropometric data in [22].

The torque and power profiles of the 10 consecutive movements are averaged to obtain intrasubject mean torque and power profiles for each initial sitting position. The experiment results for one of the sitting position are presented in Figure 14. In this figure, graphs (a) and (b) illustrate the torque and power profiles of the knee joint for the *assisted* condition (dashed lines) and the *unassisted* condition (solid lines). The thick lines represent the intrasubject mean profiles and the thin lines ±1 SD margins. The vertical line indicates the seat-off instant, which is considered to be when a sudden increase in the ground reaction force occurs, as can be observed in graph (d) of Figure 14. Graph (c) of Figure 14 shows the mean angle profiles of the knee joint. Visual comparison of the torque and power profiles of the knee joint indicates a significant reduction in the power and torque values for the *assisted* condition with respect to the *unassisted* condition.

An interpretation of the performance can be presented based on the statistical analysis of the knee joint power applied by the user for the *assisted* and *unassisted*

Table 3. Two-tailed student's *t*-test results for unassisted/assisted knee power across five different foot positions.

Foot position (cm)	−10	−7	−4	0	4
Assisted average knee power (W) (mean (SD))	7.89(1.00)	6.03(1.34)	7.23(1.21)	7.52(1.16)	7.86(1.09)
Unassisted average knee power (W) (mean (SD))	11.65(0.70)	9.85(0.66)	10.29(0.55)	10.05(0.67)	12.19(1.23)
p-value	1.77×10^{-8}	2.54×10^{-5}	2.16×10−5	6.23×10−5	9.78×10−5

Table 4. Two-tailed student's *t*-test results for unassisted/assisted knee power across four different seat heights.

Seat height (cm)	40	43	46	49
Assisted average knee power (W) (mean (SD))	7.72 (1.13)	5.77 (1.47)	6.48 (0.99)	6.8 (0.73)
Unassisted average knee power (W) (mean (SD))	11.05 (1.17)	9.66 (0.91)	8.55 (1.44)	9.97 (1.24)
p-value	4.1×10^{-4}	1.8×10^{-5}	5.6×10^{-4}	9.2×10^{-4}

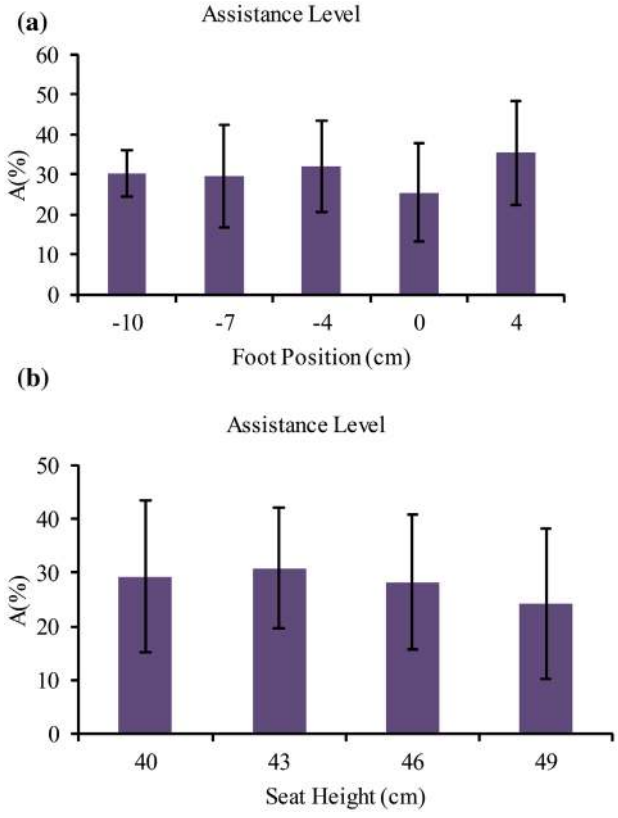

Figure 16. Average assistance level across (a) different foot positions and (b) different seat heights.

conditions across different sitting positions. To do so, the time average and standard deviations (SD) of the power profiles were calculated for all the initial sitting position under the two mentioned conditions. The results of a side-by-side comparison of the *assisted* condition with the *unassisted* condition for five different foot positions and four different seat heights are illustrated in Figures 15(a and b). In these diagrams, the bars represent mean values, and the error bars indicate the SD.

A two-tailed Student's *t*-test analysis of the *assisted* condition and the *unassisted* condition sets showed significant differences between the two conditions (p-value < 0.05) for all initial sitting positions (Tables 3 and 4). Furthermore, Figure 16 compares the effect of different foot positions and seat heights on the efficiency of the exoskeleton. In this figure, the average assistance level (A) is defined as:

$$A = \frac{\int_0^{T_f} \left(P_{\text{knee}}\right)_{unassisted} - \int_0^{T_f} \left(P_{\text{knee}}\right)_{assisted}}{\int_0^{T_f} \left(P_{\text{knee}}\right)_{unassisted}} \times 100 \quad (27)$$

where, P_{knee} is power applied by the human knee and T_f is the interval time of sit-to-stand task. Statistical significance was tested using one-way ANOVA on the assistance level and the sitting position the main factors. The ANOVA result shows no significant differences between the different experimental conditions (p-value = 0.959 for different foot position and p-value = 0.688 for different seat heights), which reveals that the assistance level was not affected by variation of the sitting position.

7. Conclusion and future works

In this paper, a novel approach for trajectory generation and control of a lower-limb exoskeleton for the application of sit-to-stand assistance is described. The trajectory generator deploys DMP theory to predict the user's intended movement based on a previously collected database of samples trajectories. An impedance controller is then used to move the exoskeleton along the predicted trajectory. The controller provides assistive torques while it allows the user to control the speed of the movement. A set of experiments were conducted on a healthy adult to assess the performance and robustness of the proposed method. The user performed several sit-to-stand movements from different sitting positions with the assistance of the exoskeleton. The results reveal that, using the proposed trajectory generation and control strategy, the exoskeleton reduces the required user's average knee power by about 30%. Moreover, the ANOVA analysis results show that there is no significant change in the performance of the controller under sitting position variations. To conclude,

the proposed method is able to efficiently assist the wearer in performing sit-to-stand movements from any sitting position in the range of the training samples.

During the experiments, it was supposed that each exoskeleton part is moving in parallel with the corresponding body part. However, a small misalignment existed which reduces the effectiveness of the exoskeleton controller. As a future work, the misalignment errors may be considered in the control process to avoid any undesirable interaction forces and to improve the exoskeleton efficiency. Furthermore, in this paper, only the sit-to-stand movement of human is studied. The proposed trajectory generation and controller can be used for both periodic and on periodic movements; therefore, as a future work the proposed method may be used to control an exoskeleton during other types of human movements such as walking, whole-body reaching, and motion transitions.

Disclosure statement

No potential conflict of interest was reported by the authors.

Notes on contributors

Kaveh Kamali received his BSc and MSc degrees in Mechanical Engineering from Ferdowsi university of Mashhad, Mashhad, Iran in 2006 and 2009, respectively. He is currently a PhD student in Mechanical Engineering Department of Ferdowsi University of Mashhad, Mashhad, Iran. His areas of research include robotics (parallel robots, wearable robots, robot calibration, micro-robotics, and rehabilitation robotics), control and smart materials.

Ali Akbar Akbari received the MSc degree in mechatronics and the PhD degree in intelligent manufacturing systems from Chiba University, Chiba, Japan in 1998 and 2003, respectively. He is currently an associate professor at the department of mechanical engineering, Ferdowsi university of Mashhad, Mashhad, Iran. His current interests include intelligent manufacturing, applied computer science, robotic and control, machine learning system, and grinding and polishing

Alireza Akbarzadeh received his PhD in Mechanical Engineering in 1997 from the University of New Mexico in USA. He worked at Motorola, USA, for 15 years where he led R&D as well as automation teams. He joined the Ferdowsi University of Mashhad in 2005 and is currently a full professor in the Mechanical Engineering Department. He has over 45 journal publications and over 60 conference papers. His areas of research include robotics (parallel robots, biologically inspired robots, bipedal robots, and rehabilitation robotics), dynamics, kinematics, control, automation, optimization as well as design, and analysis of experiments. He is also a founding member of the Center of Excellence on Soft Computing and Intelligent Information Processing (SCIIP).

References

[1] Kerr KM, White JA, Mollan RAB, et al. Rising from a chair: a review of the literature. Physiotherapy. 1991;77:15–19.

[2] Ahmad N, Ghazilla RAR, Kasi V, et al. A review on lower-limb exoskeleton system for sit to stand, ascending and descending staircase motion. Appl. Mech. Mater. 2014;541:150–1155.

[3] Mefoued S, Amirat Y, Fried G. Sit-to-stand movement assistance using an actuated knee joint orthosis. Paper presented at 4th IEEE RAS & EMBS International Conference on Biomedical Robotics and Biomechatronics (BioRob); Rome; 2012.

[4] Karavas N, Ajoudani A, Tsagarakis N, et al. Tele-impedance based assistive control for a compliant knee exoskeleton. Rob. Auton. Syst. 2015;73:78–90.

[5] Giovacchini F, Vannetti F, Fantozzi M, et al. A light-weight active orthosis for hip movement assistance. Rob. Auton. Syst. 2015;73:123–134.

[6] Dollar AM, Herr H. Lower extremity exoskeletons and active orthoses: challenges and state-of-the-art. IEEE Trans. Rob. 2008;24:144–158.

[7] Kiguchi K, Hayashi Y. An EMG-based control for an upper-limb power-assist exoskeleton robot. IEEE Trans. Syst. Man Cybern. Part B Cybern. 2012;42:1064–1071.

[8] Ijspeert AJ. Central pattern generators for locomotion control in animals and robots: a review. Neural Networks. 2008;21:642–653.

[9] Aguirre-Ollinger G. Exoskeleton control for lower-extremity assistance based on adaptive frequency oscillators: adaptation of muscle activation and movement frequency. Proc. Inst. Mech. Eng. Part H: J. Eng. Med. 2015;229:52–68.

[10] Gams A, Petric T, Debevec T, et al. Effects of robotic knee exoskeleton on human energy expenditure. IEEE Trans. Biomed. Eng. 2013;60:1636–1644.

[11] Zhang D, Hashimoto M. SBC for motion assist using neural oscillator. Paper presented at IEEE International Conference on Robotics and Automation; Kobe; 2009.

[12] Ronsse R, Koopman B, Vitiello N, et al. Oscillator-based walking assistance: a model-free approach. Paper presented at International Conference on Rehabilitation Robotics; Zurich; 2011.

[13] Ijspeert AJ, Nakanishi J, Schaal S. Learning rhythmic movements by demonstration using nonlinear oscillators. Paper presented at IEEE/RSJ International Conference on Intelligent Robots and Systems; Lausanne; 2002.

[14] Schaal S, Mohajerian P, Ijspeert A. Dynamics systems vs. optimal control – a unifying view. Prog. Brain Res. 2007;165:425–445.

[15] Ude A, Gams A, Asfour T, et al. Task-specific generalization of discrete and periodic dynamic movement primitives. IEEE Trans. Rob. 2010;26:800–815.

[16] Schultz AB, Alexander N, Ashton-Miller J. Biomechanical analyses of rising from a chair. J. Biomech. 1992;25:1383–1391.
[17] Alexander NB, Schultz AB, Warwick DN. Rising from a chair: effects of age and functional ability on performance biomechanics. J. Gerontol. 1991;46:91–98.
[18] Music J, Kamnik R, Zanchi V, et al. Human body model based inertial measurement of sit-to-stand motion kinematics. WSEAS Trans. Syst. 2008;7:156–164.
[19] Schaal S, Atkeson CG. Constructive incremental learning from only local information. Neural Comput. 1998;10:2047–2084.
[20] Shepherd RB, Koh HP. Some biomechanical consequences of varying foot placement in sit-to-stand in young women. Scand. J. Rehabil. Med. 1996;28: 79–88.
[21] Khemlani MM, Carr JH, Crosbie WJ. Muscle synergies and joint linkages in sit-to-stand under two initial foot positions. Clin. Biomech. 1999;14:236–246.
[22] NASA: NASA-STD-3000, Man–systems integration standards, vol. 1 [Internet]. Houston: NASA Johnson Space Center; Available from: http://msis.jsc.nasa.gov/.